Proceedings of the Combustion Institute 41 (2025) 105903

Contents lists available at ScienceDirect

Proceedings of the Combustion Institute

journal homepage: www.elsevier.com/locate/proci

Numerical investigation of hot-spot surface ignition of hydrogen-air mixtures

Hongchao Chu *, Tiankai Li, Haogeng Bai, Zezheng Li, Heinz Pitsch

Institute for Combustion Technology, RWTH Aachen University, Aachen, 52056, Germany

ARTICLE INFO

Keywords:
Hydrogen
Hot-spot surface ignition
Premixed
Differential diffusion
Soret effect

ABSTRACT

The analysis of hot-spot surface ignition is critical for ensuring the safety, operational stability, and efficiency of a wide range of combustion devices. In this study, direct numerical simulations (DNS) of hot-spot surface ignition of quiescent hydrogen-air mixtures were performed. A wide range of parameter variations was explored, including changes in fuel-air equivalence ratio, unburned gas temperature, pressure, hot-spot size on the wall, and wall surface catalytic reactivity. In addition, the impacts of differential diffusion and Soret effects on the hot-spot surface ignition were assessed by employing different species transport assumptions in the simulation. It was found that for a given mixture, ignition is achievable only if the size of the wall-heated gas in the direction parallel to the wall exceeds a critical ignition radius, similar to the ignition of a spherical flame in homogeneous mixtures without wall effects. The thickness of the thermal boundary layer perpendicular to the wall has no significant influence on ignition occurrence. In addition, the ignition occurrence and ignition delay time were found to be affected by differential diffusion through two distinct mechanisms. Ignition occurrence is determined by the impacts of differential diffusion on the critical ignition radius, which arise from the complex interactions of chemistry, mass transfer, and heat transfer, and strongly depend on the fuel-air equivalence ratio. In contrast, ignition delay time is primarily affected by the diffusion of the H radical, where faster diffusion leads to a longer delay. The comparison between the inert wall and an infinitely fast catalytic wall further highlights the significance of radical concentrations.

1. Introduction

For the transition to a sustainable energy system, green hydrogen has emerged as a promising energy carrier, particularly for the sectors that are difficult to electrify [1]. The use of hydrogen as a fuel in domestic and industrial burners and in internal combustion engines (ICE) of heavy-duty vehicles is expected to significantly facilitate the decarbonization of these applications [2]. However, the distinctly different combustion properties of hydrogen compared to conventional hydrocarbon fuels present various challenges. In particular, the use of hydrogen as a fuel in burners and ICE can lead to harmful combustion phenomena, such as flashback [3–6] in the former and pre-ignition [7,8] in the latter. Ignition on a hot surface has been identified as one of the initiation mechanisms for both flashback [9] and pre-ignition [8,10]. This study focuses on the hot-spot surface ignition of hydrogen-air mixtures, which is important not only for the utilization of hydrogen in burners and ICE but also for the safety concerns of accidental hydrogen leakage.

In the literature, the surface ignition of various gases and liquid fuels has been studied both experimentally and numerically [11–18]. Research has focused on the response of the minimum surface temperature required for successful ignition and the ignition delay time (IDT) to factors such as the fuel-air equivalence ratio [11,12,15], gas flow velocity and residence time [11,12], hot-spot size [11,18], pressure [12,15], preheating [12], surface materials and their catalytic reactivity [11,13,16], and fuel type [14]. In addition, the effects of buoyancy-induced convection on the ignition dynamics initiated by a glow plug have been discussed [17]. However, several fundamental aspects of hydrogen-air mixture ignition on hot surfaces are yet to be addressed. In particular, it is well known that for the successful ignition of gas mixtures by a spherical energy source without wall effects, a critical radius must be exceeded [19,20]. However, it remains unclear whether this principle also applies to hot-spot surface ignition and whether it is the size of the hot spot on the surface or the thickness of the thermal boundary layer perpendicular to the surface that must exceed a critical value. In addition, differential diffusion and Soret effects have been found to significantly impact hydrogen flames, including flame-wall interactions [3], minimum ignition energy [19,21], and flame kernel development [22]. In particular, the hydrogen accumulation in hot gas regions or near the hot wall due to the Soret effect was found to significantly influence the flame behavior [3,23–25]. Therefore, assessing the influence of differential diffusion and Soret

* Corresponding author.
E-mail address: h.chu@itv.rwth-aachen.de (H. Chu).

https://doi.org/10.1016/j.proci.2025.105903
Received 30 April 2025; Accepted 21 September 2025
Available online 18 October 2025

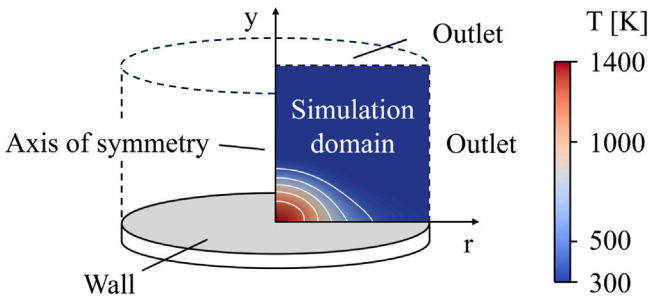

Fig. 1. Numerical configuration and boundary conditions.

effect on the ignition of hydrogen-air mixtures on hot surfaces is of significant interest.

This paper aims to address the above-mentioned questions through direct numerical simulations (DNS). A series of two-dimensional DNS using detailed chemical kinetics has been performed, employing a wide range of parameters, including variations in fuel-air equivalence ratio, unburned gas temperature, pressure, hot-spot size on the wall, and wall catalytic reactivity. The influence of differential diffusion and the Soret effect is separately assessed by employing different species transport assumptions in the DNS. Due to the wide range of parameter variations and the complex interactions of wall effects, heat and mass transfer, and chemistry, a quiescent initial condition without flow is considered. Effects of laminar and turbulent flows are the subject of future study. The analysis primarily focuses on the occurrence of ignition and the ignition delay time.

2. Configuration and numerical methods

2.1. Configuration

Due to the axisymmetric flame configuration, two-dimensional simulation domains and cylindrical coordinates are employed. The numerical configuration, including the boundary conditions, is shown in Fig. 1. The wall temperature T_{wall} is specified to exhibit a hot spot and vary smoothly in space, as given by

$$T_{\mathrm{wall}} = T_{\mathrm{u}} + (T_{\mathrm{max}} - T_{\mathrm{u}}) \cdot \exp(-\frac{r^2}{2R^2}), \tag{1}$$

where T_{u} is the unburned gas temperature, T_{max} the maximum wall temperature, r the radial coordinate, and R the hot-spot size. To facilitate ignition within a reasonable time frame and to minimize computational costs, a relatively high wall temperature of $T_{\mathrm{max}} = 1400$ K is selected in this study, which aligns with the previous studies [15, 17]. Homogeneous quiescent fuel-air mixtures are specified as initial condition.

The simulations conducted are summarized in Table 1. The cases are named according to their initial conditions and numerical setup. For instance, the case 'P1T300LexSI' represents an initial condition with a pressure of 1 bar and an unburned gas temperature of 300 K. Further, 'x' indicates that the non-unity Lewis numbers (Le) of individual species are considered, while 'S' and 'I' denote the inclusion of the Soret effects and an inert wall, respectively. Here, the Lewis numbers of individual species are kept constant and derived from the burned gas of the corresponding unstretched laminar flames. It is worth noting that for all the cases in Table 1, parameter variations of fuel-air equivalence ratio $\phi \in [0.3, 0.5, 0.7, 1.0, 2.0]$ and hot-spot size $R/l_{\mathrm{f,min}} \in [0.2, 0.5, 1.0, 2.0, 4.0, \infty]$ are conducted. These variations in R are chosen so that both ignition and no-ignition cases can be observed under the given thermodynamic conditions. This implies that the case 'P1T300LexSI', for example, comprises 30 simulations. Here, $l_{\mathrm{f,min}}$ represents the minimum unstretched flame thickness across different equivalence ratios (ϕ) for each combination of pressure (p) and unburned gas temperature (T_{u}). The flame thickness l_{f} is computed from the maximum temperature gradient. To ensure consistency in comparisons, when modifying the species transport assumptions or wall catalytic reactivity, the values of $l_{\mathrm{f,min}}$ are taken from the corresponding reference cases with names ending in 'LexSI'. The flame thickness for all cases, covering various ϕ, is provided in the supplementary material (Table S-1). For $R = \infty$, the simulation reduces to a 1D problem. In total, 425 2D and 85 1D simulations were conducted. The parameter variations in thermodynamic conditions include the typical conditions for residential burners ((1 bar, 300 K) and (1 bar, 500 K)), intake stroke of turbocharged hydrogen engines ((1.5 bar, 300 K) and (2 bar, 300 K)), and compression stroke of turbocharged hydrogen engines ((5 bar, 423 K) and (10 bar, 516 K)). Since pre-ignition in hydrogen engines typically occurs at pressures below 10 bar [26], higher pressures are not considered. To investigate the differential diffusion effects, the Lewis numbers of all species are set to unity and two for the cases 'P1T300Le1NoSI' and 'P1T300Le2NoSI', respectively. The Soret effect is disabled in the cases 'P1T300LexNoSI', 'P1T300Le1NoSI', and 'P1T300Le2NoSI'. To assess the catalytic effects of the wall, the infinitely fast heterogeneous catalysis (IFHC) model for surface reactions proposed by De Nardi et al. [27] is employed in the cases with names ending in 'N' (non-inert), representing the extreme scenario of infinitely fast catalysis. This complements the opposite extreme of the inert wall assumption considered in the other cases. Unlike simply setting the radical concentration on the surface to zero, IFHC ensures element conservation during radical recombination on the surface. Further, isobaric auto-ignition and forced spherical ignition of homogeneous mixtures without wall effects are also simulated as references for comparison.

Table 1
Overview of the simulations.

Case name	p [bar]	T_{u} [K]	Le [–]	Soret [–]	Wall [–]	$l_{\mathrm{f,min}}$ [μm]
P1T300LexSI	1	300	x	Yes	inert	329
P1T300LexSN	1	300	x	Yes	non-inert	329
P1T500LexSI	1	500	x	Yes	inert	387
P1T500LexSN	1	500	x	Yes	non-inert	387
P2T300LexSI	2	300	x	Yes	inert	142
P2T300LexSN	2	300	x	Yes	non-inert	142
P2T500LexSI	2	500	x	Yes	inert	170
P2T500LexSN	2	500	x	Yes	non-inert	170
P1.5T300LexSI	1.5	300	x	Yes	inert	201
P1.5T300LexSN	1.5	300	x	Yes	non-inert	201
P5T423LexSI	5	423	x	Yes	inert	55
P5T423LexSN	5	423	x	Yes	non-inert	55
P10T516LexSI	10	516	x	Yes	inert	26
P10T516LexSN	10	516	x	Yes	non-inert	26
P1T300LexNoSI	1	300	x	No	inert	329
P1T300Le1NoSI	1	300	1	No	inert	329
P1T300Le2NoSI	1	300	2	No	inert	329

2.2. Numerical methods

The governing equations and the numerical methods used in this study are the same as the previous studies [28,29]. The Soret effect is included following Zhou et al. [30] and Schlup et al. [31] with a mixture-averaged thermal diffusion model. The chemical reactions are described with a detailed mechanism proposed by Panigrahy et al. [32], which has been validated with experiments under different conditions. The ideal gas law is used as the equation of state. In the DNS, the low-Mach number limit [33] is employed for the reacting flow. The diffusive scalar transport is described using the Curtiss-Hirschfelder approximation [34]. The diffusivity of species i is determined by $D_{\mathrm{i}} = \lambda/(\rho c_{\mathrm{p}} Le_{\mathrm{i}})$, where λ is the mixture thermal conductivity, and ρ and c_{p} are the mixture density and specific heat capacity at constant pressure, respectively. Le_{i} denotes the Lewis number of species i. The numerical schemes used in this study are the same as those in previous works [28,

29] and are therefore not repeated here. However, they are provided in the supplementary material for convenient reference.

The simulation domain is specified to be sufficiently large, with a size of at least $3R$. The numerical cell size is selected to satisfy $\Delta x \leq l_{\mathrm{f,min}}/20$, ensuring sufficient resolution of both the wall thermal boundary layer and the flame. A time step size of 0.0025 to 0.5 μs is chosen, such that the formation of the thermal boundary layer due to wall heating and the ignition process are adequately resolved. Simulations were performed in most cases until ignition occurs. For cases without successful ignition, simulations were performed for a duration of at least five times the longest ignition delay among the 30 simulations within the same case group, such as 'P1T300LexSI' in Table 1. Near the end of the simulation, the scalar fields exhibit nearly no variation over time.

3. Results and discussion

3.1. Ignition dynamics

This section examines the dynamics of successful and failed ignition. Fig. 2(a) shows the temperature distribution at various time instances for two cases with (left) and without (right) successful ignition. A criterion for successful ignition is introduced in the following. The white lines represent the temperature iso-line at $T = 800$ K. $R_{\mathrm{f,r}}$ and $R_{\mathrm{f,y}}$ denote the size of the hot-gas region in the directions parallel and perpendicular to the wall, respectively, which changes with time. The successful ignition case belongs to 'P1T300LexSI', while the no-ignition case belongs to 'P1T300Le1NoSI'. Both cases have $\phi = 0.3$ and $R = l_{\mathrm{f,min}}$. The thermal boundary layer initially expands over time, particularly in the direction perpendicular to the wall, due to the heating effect from the hot wall. In the case of successful ignition, the flame initiates within the thermal boundary layer at 0.16 ms and subsequently propagates away from the wall. After ignition, the temperature of the burned gas surpasses that of the wall, resulting in heat loss to the wall. In the case without ignition, the thermal boundary layer initially expands and then remains nearly unchanged over time. In Fig. 2(b), $R_{\mathrm{f,y}}$ for the case with ignition at 0.16 ms is slightly lower than that of the case without ignition. This is caused by the differences in the heat release rates between the two cases due to the different Lewis number assumptions. A detailed explanation for this is provided in the supplementary material. In this study, the evolution of $R_{\mathrm{f,r}}$ is used to quantitatively differentiate between cases with and without successful ignition. As shown in Fig. 2(b), for the case with successful ignition, $R_{\mathrm{f,r}}$ increases continuously after ignition due to flame propagation. In contrast, for the case with no ignition, $R_{\mathrm{f,r}}$ does not change significantly with time. Similar to the definition of ignition delay time for auto-ignition in gas mixtures without wall effects [35,36], hot-spot surface ignition is defined as the moment when the OH mass fraction reaches 10% of its peak value after ignition. For the case with successful ignition, the ignition moment is also illustrated in Fig. 2(b) by the vertical dashed line, occurring slightly before the significant increase of $R_{\mathrm{f,r}}$.

3.2. Ignition occurrence

A central question in this study is whether hot-spot surface ignition can occur under specific thermodynamic conditions for various hot-spot sizes. This is shown in Fig. 3, where cases with ignition are marked with green circles, while cases without ignition are marked with red crosses. The hot-spot size significantly impacts the occurrence of ignition, with larger hot spots facilitating ignition as shown in Fig. 3(a). All the cases with infinitely large hot spots are successfully ignited. As expected, mixtures closer to stoichiometry are more likely to be ignited. The impact of differential diffusion and Soret effects is demonstrated by comparing Fig. 3(a), (b), (c) and (d). The Soret effect significantly increases the hydrogen concentration near the wall, as shown in the supplementary material (Fig. S-2). Its impact on ignition occurrence is demonstrated by the cases 'P1T300LexSI' (Fig. 3(a)) and 'P1T300LexNoSI' (Fig. 3(b)) with $R = 1l_{\mathrm{f,min}}$ and $\phi = 2$. The Soret effect prevents ignition in the rich mixture. Since the results in both cases show little sensitivity to ϕ under the investigated conditions, the Soret effect has no noticeable impact on ignition occurrence for other ϕ and R values. Interestingly, differential diffusion has a significant impact on ignition occurrence. In the case 'P1T300Le1NoSI', differential diffusion and Soret effects are disabled. Compared to this case, differential diffusion in 'P1T300LexNoSI' (Fig. 3(b)) promotes ignition in extreme lean hydrogen-air mixtures while suppressing it in slightly lean and rich mixtures. When the Lewis numbers of all species are set to two (Fig. 3(d)), both lean and rich cases become harder to ignite, compared to the corresponding cases without differential diffusion (Fig. 3(c)).

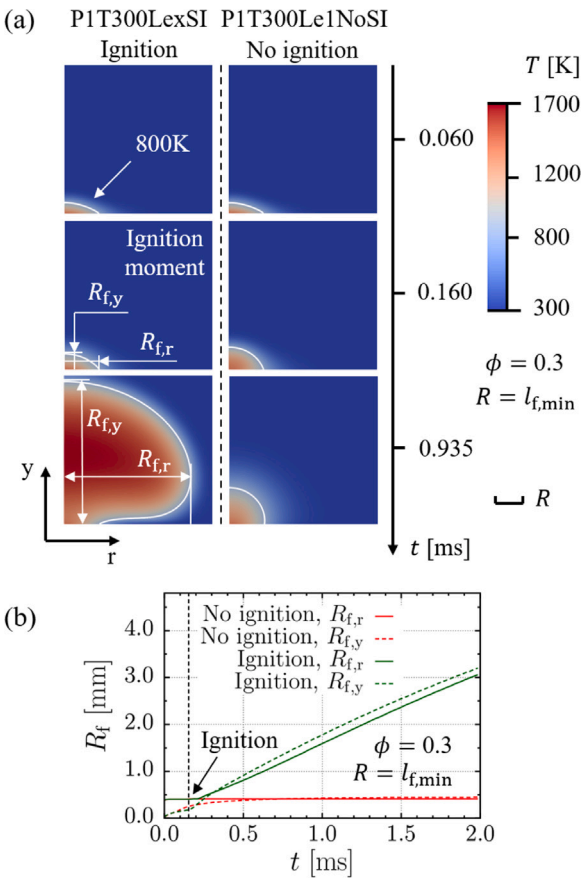

Fig. 2. (a) Typical temperature field evolution for cases with (left) and without (right) successful ignition. R: size of the hot spot in Eq. (1). Different species transport assumptions are employed in the left (P1T300LexSI) and the right (P1T300Le1NoSI) cases, as listed in Table 1. To enhance comparability, only a portion of the simulation domain is displayed. (b) Evolution of the corresponding size of the hot-gas region in the directions parallel ($R_{\mathrm{f,r}}$) and perpendicular ($R_{\mathrm{f,y}}$) to the wall.

Increasing the unburned gas temperature improves the likelihood of ignition, as illustrated by comparing Fig. 3(a) and (e). Conversely, higher pressures inhibit ignition, as observed by comparing Fig. 3(a) and (f). Note that the minimum flame thickness, $l_{\mathrm{f,min}}$, decreases drastically with increasing pressure, as shown in Table 1. For the same absolute value of R, the high-pressure case is more likely to ignite, as illustrated by comparing $R = 2l_{\mathrm{f,min}}$ in Fig. 3(f) and $R = 0.5l_{\mathrm{f,min}}$ in Fig. 3(e). The former, at a higher pressure, has a smaller hot-spot size of $R = 52$ μm but still results in successful ignition for stoichiometric mixtures. In contrast, the latter, at a lower pressure, exhibits a larger hot-spot size of $R = 194$ μm but fails to ignite for stoichiometric mixtures.

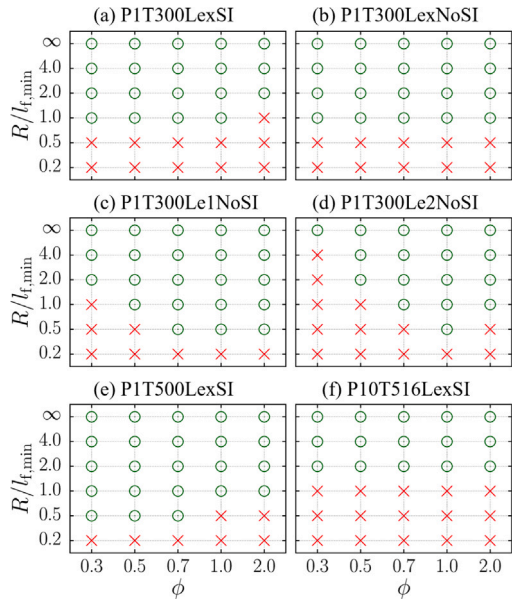

Fig. 3. Occurrence of ignition under different conditions. To enhance clarity, cases with ignition are marked with green circles, while cases without ignition are marked with red crosses.

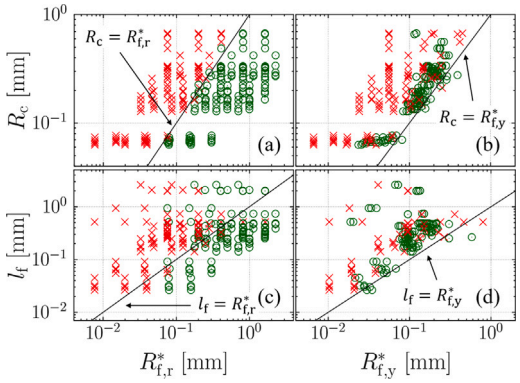

Fig. 4. Comparisons between the size of the thermal boundary layer ($R^*_{f,r}$ and $R^*_{f,y}$) and the flame characteristic lengths (l_f and R_c) for all the cases in Table 1 with the inert wall.

These observed trends align with previous studies [11,12,15,18], which reported the impacts of gas temperature and pressure on the ignition delay time or the critical wall temperature for successful ignition.

Inspired by the effects of R on ignition occurrence discussed above, and considering the concept of the critical ignition radius, it is of interest to determine whether it is the size of the thermal boundary layer parallel to the surface or its thickness perpendicular to the surface that must exceed a critical value for successful ignition. The size of the thermal boundary layer is characterized by the radius $R_{f,r}$ and thickness $R_{f,y}$ as shown in Fig. 2(a). Here, the temperature iso-line of 800 K is chosen, which is slightly lower than the typical critical wall temperature for successful ignition in previous studies [16,37]. Since $R_{f,r}$ and $R_{f,y}$ are time-dependent, for cases with successful ignition, the values are taken at the time of ignition. For cases without ignition, the values are recorded at the end of the simulation, when $R_{f,r}$ and $R_{f,y}$ do not change with time. The evaluated quantities are denoted as $R^*_{f,r}$ and $R^*_{f,y}$, respectively. According to Kalghatgi and Bradley [8], we consider two characteristic flame length scales: the thickness of the unstretched flame, l_f, and the critical ignition radius, R_c, for ignition by a spherical energy source in the absence of wall effects. The determination of R_c is detailed in the supplementary material. To also account for differential diffusion effects in R_c, the same species transport assumptions as those in the hot-spot surface ignition simulations are applied in the corresponding simulations used to determine R_c. Fig. 4 compares the above-mentioned length scales for all the cases in Table 1 with the inert wall. It is evident that the critical ignition radius, R_c, and the size of the thermal boundary layer parallel to the wall, $R^*_{f,r}$, are the key factors. With the exception of few outliers, ignition occurs when $R^*_{f,r}$ exceeds R_c. It is a remarkable finding that this relationship holds across a wide range of variations, including thermodynamic conditions of the unburned gas and different species transport assumptions. This indicates that the existing theory and numerical methods developed to predict the critical radius for spherical flame ignition in homogeneous mixtures without wall effects, such as in [19–21], can be analogously applied to predict the critical hot-spot size for surface ignition. R_c without wall effects can be determined either from theoretical analysis [19] or from 1D simulations with spherical coordinates, which require significantly fewer computational resources than 3D or 2D simulations with a hot-spot surface. The observed outliers may arise from differences in the configurations of spherical flame ignition and hot-spot surface ignition. It is worth noting that the ratio of flame thickness l_f to the thermal boundary layer size $R^*_{f,r}$ can also reflect the tendency of hot-spot surface ignition to some extent, as also reported by Kalghatgi and Bradley [8]. It is essential to recognize that R_c is smaller than 1 mm under the investigated conditions, which is an order of magnitude smaller than that of conventional hydrocarbon fuels [38]. This is consistent with the high propensity for pre-ignition in hydrogen engines. It should be emphasized that R_c for the ignition of gas mixtures without wall effects increases with lower peak gas temperatures, as shown in the study by Chi et al. [20]. The same trend is also observed for hot-spot surface ignition. Simulation results with a lower wall temperature (1000 K) are provided in the supplementary material (Fig. S-11-13). These cases are harder to ignite and exhibit larger values of R_c. The results with the lower wall temperature align with the main findings discussed here.

3.3. Ignition delay time

Practical applications exhibit various flow configurations and residence times. Hot-spot surface ignition can be avoided if the residence time is small compared to the ignition delay time. Therefore, it is of practical importance to examine the ignition delay time of hot-spot surface ignition. Fig. 5 illustrates how the ignition delay time responds to various factors, including the fuel-air equivalence ratio, pressure, unburned gas temperature, hot-spot size, and species transport assumptions. For comparison, the auto-ignition delay time of homogeneous mixtures without wall effects, denoted as '0D', is also presented. In these 0D simulations, the initial unburned gas temperature is set to the maximum wall temperature (1400 K). As depicted in Fig. 5(a), IDT of the hot-spot surface ignition is relatively insensitive to variations in the fuel-air equivalence ratio, aligning with the responses of IDT_{0D} to ϕ. This is consistent with the previous study by Chi et al. [20]. It is worth noting that the IDT of hot-spot surface ignition is significantly larger than IDT_{0D}. This can be attributed to heat loss to the surrounding low-temperature gases, which is absent during the auto-ignition of homogeneous mixtures. Fig. 5(b) shows the impact of the hot-spot size. The same trend is observed in other cases with elevated pressure and temperature, as well as different species transport assumptions. These results are provided in the supplementary material (Fig. S-4 and 5). As shown in Fig. 5(a) and (b), an increase in unburned gas temperature, pressure, or hot-spot size reduces the ignition delay time. These trends are consistent with previous studies [11,12,15]. Note that the pressure dependence may vary under different conditions.

The influence of differential diffusion and Soret effects on IDT is illustrated in Fig. 5(c). Since transport properties do not affect the corresponding IDT_{0D}, it remains the same across the cases with different species transport assumptions. Despite the observed influence of the

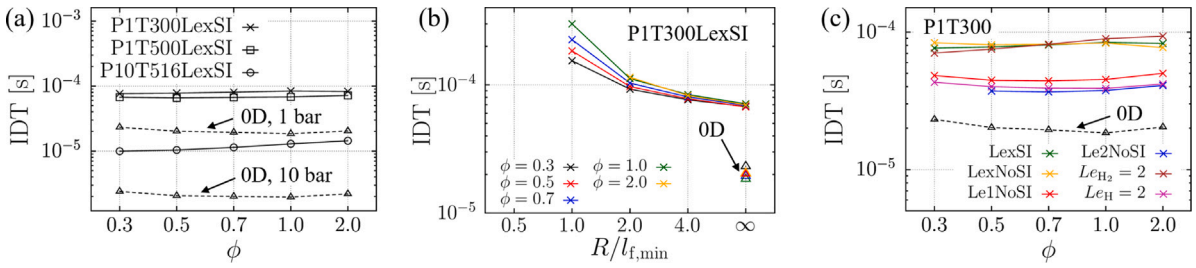

Fig. 5. Dependence of ignition delay time on the thermodynamic state of unburned gas (a), hot-spot size (b), and species transport assumptions (c). In sub-figures (a) and (c), only cases with $R = 4l_{f,min}$ are presented. The same trend is observed for the other hot-spot sizes.

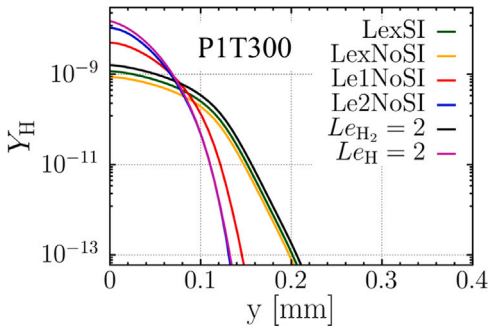

Fig. 6. Distribution of H radical mass fraction as a function of distance from the wall along the y-axis through the hot-spot center for $R = 4l_{f,min}$ and $\phi = 1.0$ before ignition ($t = 0.01$ ms).

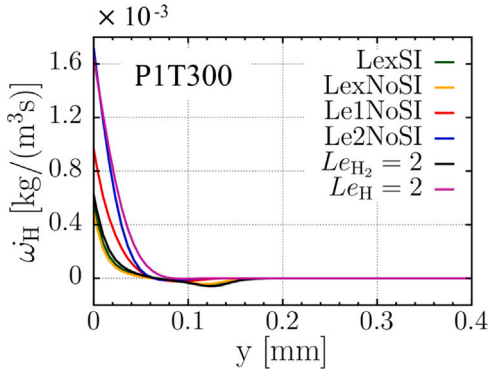

Fig. 7. Distribution of the chemical source term of H radical as a function of distance from the wall along the y-axis through the hot-spot center for $R = 4l_{f,min}$ and $\phi = 1.0$ before ignition ($t = 0.01$ ms).

Soret effect on ignition occurrence in Fig. 3(a) and (b), its impact on the IDT of hot-spot surface ignition is negligible. However, differential diffusion has a significant effect on the IDT. Unlike its influence on ignition occurrence, which depends on ϕ (Fig. 3(a) and (d)), the impact of differential diffusion on IDT is nearly independent of ϕ. Setting the Lewis numbers to unity or two significantly reduces the IDT for different ϕ values. To further investigate the effects of differential diffusion on IDT, additional simulations are conducted. In these cases, the Lewis numbers of H_2 (Le_{H_2}) or the radical H (Le_H) are set to two. As shown in Fig. 5(c), the IDT for $Le_{H_2} = 2$ is similar to that of the 'LexSI' case. In contrast, the IDT for $Le_H = 2$ closely resembles that of the 'Le2NoSI' case. The same trend was observed for other hot-spot sizes, which is shown in the supplementary material (Fig. S-6). This indicates that the transport of H radical is particularly critical.

Fig. 6 presents the spatial distributions of the mass fraction of H radical as a function of distance from the wall along the y-axis through the hot-spot center for $R = 4l_{f,min}$ and $\phi = 1.0$ before ignition ($t = 0.01$ ms) for cases with different species transport assumptions. The spatial distributions of the H radical in the 'P1T300LexSI' and 'P1T300LexNoSI' cases are almost identical, indicating that the Soret effect has a negligible impact. However, the Lewis number plays a crucial role in determining the H radical distribution. As shown in Fig. 6, for larger Lewis numbers, the H radical exhibits a more concentrated distribution near the wall due to its lower diffusivity, given by $D_H = \lambda/(\rho c_p Le_H)$, where λ is the mixture thermal conductivity, ρ is the mixture density, and c_p is the mixture heat capacity at constant pressure. The corresponding distributions of the chemical source term of H radical are provided in Fig. 7. Most of the H radicals are generated near the wall, where the temperature is high. The behavior in Figs. 3 and 5 is a remarkable finding, indicating that differential diffusion influences ignition occurrence and IDT through different mechanisms. Ignition occurrence is determined by the critical ignition radius, which arises from the complex interactions between chemical kinetics and transport processes, and is significantly influenced by the fuel-air equivalence ratio ϕ. However, IDT is mainly governed by the diffusion of the H radical. Higher diffusivity of the H radical tends to increase the IDT, regardless of the value of ϕ.

3.4. Impact of wall catalytic reactivity

As discussed in Section 3.3, the radical concentration significantly influences the ignition delay time. Since radicals can be consumed by the recombination on the wall, the wall catalytic reactivity is expected to significantly influence the hot-spot surface ignition. To investigate this effect, the following compares results obtained using the IFHC wall model [27] with those using the inert wall assumption. The IFHC model introduces three infinitely fast catalytic reactions on the wall surface, which consume the H, O, and OH radicals while maintaining element balance. A detailed description of the IFHC model can be found in [27]. The model is applied to cases where differential diffusion and the Soret effect are considered.

Assuming the IFHC wall notably reduces the radical concentration near the wall surface, as shown in the supplementary material (Fig. S-10). The ignition occurrence and IDT with the IFHC wall are shown in Fig. 8. As expected, the non-inert wall inhibits the occurrence of ignition, as can be observed by comparing the behavior for $R = l_{f,min}$ in Fig. 8(a) with that in Fig. 3(a). The same effects of the catalytic wall can also be found for other conditions, which is shown in the supplementary material (Fig. S-8). The comparison between $R^*_{f,r}$ and R_c is shown in Fig. 8(b). All the cases in Table 1 with the non-inert wall are presented. Note that wall catalytic reactivity has no significant effect on $R^*_{f,r}$, as demonstrated in the supplementary material (Fig. S-9). Additionally, R_c is also unaffected since wall effects are not considered when determining R_c. However, comparing $R^*_{f,r}$ and R_c still provides valuable insights into the likelihood of ignition occurrence. In particular, the boundary between ignited and non-ignited cases is approximately parallel to the line $R_c = R^*_{f,r}$. Therefore, the critical ignition radius remains a valuable length scale for estimating the required hot-gas size for successful surface ignition. As shown in Fig. 8(c), the IFHC wall significantly increases the IDT (by a factor up to five), which is attributed to the radical consumption on the wall. This aligns with the discussion in Section 3.3 and the trends reported in the literature [11,16].

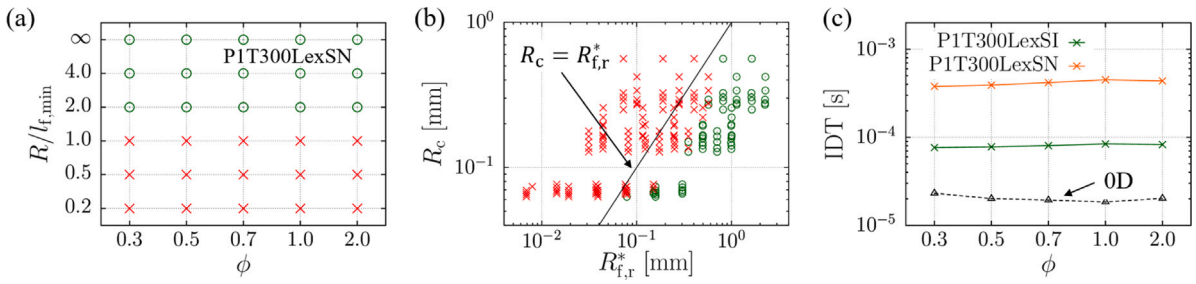

Fig. 8. Impact of wall catalytic reactivity: (a) ignition occurrence, (b) comparison of R_c and $R^*_{f,r}$, and (c) ignition delay time.

4. Conclusions

Direct numerical simulations of hot-spot surface ignition of hydrogen-air mixtures are presented. The impacts of differential diffusion and Soret effects are assessed by employing different species transport assumptions in the simulation. Further, a wide range of parameter variations is explored, including changes in fuel-air equivalence ratio, unburned gas temperature, pressure, the hot-spot size on the wall, and wall catalytic reactivity. Impacts of these parameters on the ignition occurrence and ignition delay time are comprehensively investigated.

Under a given thermodynamic condition, ignition occurrence depends on the size of the hot spot. It is found that the critical ignition radius R_c and the size of the hot gas parallel to the wall $R^*_{f,r}$ are crucial. In contrast, the thickness of the thermal boundary layer perpendicular to the wall has no significant influence on ignition. Ignition occurs only if $R^*_{f,r}$ exceeds R_c, similar to the ignition of spherical flames in homogeneous mixtures without wall effects. Interestingly, differential diffusion is found to influence ignition occurrence and delay time through different mechanisms. The former is governed by a characteristic length scale, the critical ignition radius, which results from the complex interactions of chemistry, mass transfer, and heat transfer, and depends strongly on thermodynamic conditions, particularly the fuel-air equivalence ratio, ϕ. The latter is primarily affected by the diffusion of the H radical, where faster diffusion leads to longer ignition delay time, independent of ϕ. In addition, the impact of the wall catalytic reactivity is analyzed. In particular, the ignition delay time increases by up to a factor of five. This further highlights the significance of radical concentrations. The infinitely fast catalytic wall exhibits strong inhibitory effects on the ignition. Even though ignition occurrence is significantly influenced by the catalytic effects of the wall, the critical ignition radius remains a valuable length scale for estimating the required hot-gas size for successful surface ignition.

Novelty and significance statement

The novelty of this research lies in the quantitative analysis of the governing length scales for hot-spot surface ignition, the assessment of the roles of differential diffusion and the Soret effect in the ignition of hydrogen–air mixtures, and the identification of two distinct mechanisms through which differential diffusion influences ignition occurrence and delay time, respectively, in hot-surface-induced ignition. This is significant from both fundamental and practical perspectives, as hot-spot surface ignition has been identified as one of the initiation mechanisms for flashback in hydrogen burners and pre-ignition in hydrogen engines. These phenomena constrain the practical use of hydrogen in such devices, despite the promise of hydrogen as a fuel for sustainable, carbon-free energy systems.

CRediT authorship contribution statement

Hongchao Chu: Conceptualization, Data curation, Formal analysis, Writing. **Tiankai Li:** Data curation, Formal analysis, Reviewing, Editing. **Haogeng Bai:** Data curation, Formal analysis, Reviewing, Editing. **Zezheng Li:** Data curation, Formal analysis, Reviewing, Editing. **Heinz Pitsch:** Conceptualization, Formal analysis, Supervision, Reviewing, Editing.

Declaration of competing interest

The authors declare that they have no known competing financial interests or personal relationships that could have appeared to influence the work reported in this paper.

Acknowledgments

H. C. and H. P. acknowledge the funding by the German Federal Ministry of Education and Research (Bundesministerium für Bildung und Forschung, BMBF) via the HyInnoICE project as a part of the Hydrogen Clusters4Future (Zukunftscluster Wasserstoff). H. B. and H. P. acknowledge the funding by the Deutsche Forschungsgemeinschaft (DFG, German Research Foundation), Germany under Research Unit FOR2687 with project number 349537577. The authors gratefully acknowledge the computing time provided to them at the NHR Center NHR4CES at RWTH Aachen University, Germany (project number p0021021). This is funded by the Federal Ministry of Education and Research, Germany, and the state governments participating on the basis of the resolutions of the GWK for national high performance computing at universities (www.nhr-verein.de/unsere-partner).

Appendix A. Supplementary data

Supplementary material related to this article can be found online at https://doi.org/10.1016/j.proci.2025.105903.

References

[1] H. Pitsch, The transition to sustainable combustion: Hydrogen- and carbon-based future fuels and methods for dealing with their challenges, Proc. Combust. Inst. 40 (2024) 105638.
[2] M.A. Habib, G.A. Abdulrahman, A.B. Alquaity, N.A. Qasem, Hydrogen combustion, production, and applications: A review, Alex. Eng. J. 100 (2024) 182–207.
[3] F. Fruzza, H. Chu, R. Lamioni, T. Grenga, C. Galletti, H. Pitsch, The importance of Soret effect, preferential diffusion, and conjugate heat transfer for flashback limits of hydrogen-fueled perforated burners, Proc. Combust. Inst. 40 (2024) 105581.
[4] H. de Vries, A.V. Mokhov, H.B. Levinsky, The impact of natural gas/hydrogen mixtures on the performance of end-use equipment: Interchangeability analysis for domestic appliances, Appl. Energy 208 (2017) 1007–1019.
[5] E. Flores-Montoya, A. Aniello, T. Schuller, L. Selle, Predicting flashback limits in H2 enriched CH4/air and C3H8/air laminar flames, Combust. Flame 258 (2023) 113055.

[6] F. Vance, L. de Goey, J. van Oijen, Development of a flashback correlation for burner-stabilized hydrogen-air premixed flames, Combust. Flame 243 (2022) 112045.
[7] M. Yeganeh, K. Rönn, S. Karimkashi, Q. Cheng, P. Hlaing, J. Hyvönen, V. Vuorinen, O. Kaario, M. Larmi, Experimental investigations of hydrogen pre-ignition phenomenon induced by two different lubricating oils in a rapid compression expansion machine, Proc. Combust. Inst. 40 (2024) 105715.
[8] G.T. Kalghatgi, D. Bradley, Pre-ignition and 'super-knock' in turbo-charged spark-ignition engines, Int. J. Engine Res. 13 (2012) 399–414.
[9] H. Pers, A. Aniello, F. Morisseau, T. Schuller, Autoignition-induced flashback in hydrogen-enriched laminar premixed burners, Int. J. Hydrog. Energy 48 (2023) 10235–10249.
[10] L. Bates, D. Bradley, G. Paczko, N. Peters, Engine hot spots: Modes of auto-ignition and reaction propagation, Combust. Flame 166 (2016) 80–85.
[11] T. Sano, A. Yamashita, Flame ignition of premixed methane air mixtures on a high-temperature plate, JSME Int. J. Ser. B 37 (1994) 180–186.
[12] M. Ziauddin, A. Balakrishna, D. Vlachos, L. Schmidt, Ignition of methane flames in oxygen near inert surfaces: Effects of composition, pressure, preheat, and residence time, Combust. Flame 110 (1997) 377–391.
[13] N. LaPointe, C. Adams, J. Washington, Hot surface ignition of gasoline on engine materials, SAE Tech. Pap. (2006).
[14] V. Somandepalli, S. Kelly, S. Davis, Hot surface ignition of ethanol-blended fuels and biodiesel, in: SAE World Congress & Exhibition, 2008.
[15] S.K. Menon, P.A. Boettcher, B. Ventura, G. Blanquart, Hot surface ignition of n-hexane in air, Combust. Flame 163 (2016) 42–53.
[16] R. Mével, J. Melguizo-Gavilanes, L. Boeck, J. Shepherd, Experimental and numerical study of the ignition of hydrogen-air mixtures by a localized stationary hot surface, Int. J. Heat Fluid Flow 76 (2019) 154–169.
[17] L. Boeck, J. Melguizo-Gavilanes, J. Shepherd, Hot surface ignition dynamics in premixed hydrogen–air near the lean flammability limit, Combust. Flame 210 (2019) 467–478.
[18] R.K. Velamati, S. Raj, P. Parthasarathy, J.E. Veetil, Ignition studies of hydrogen-air mixtures over hot wire, Int. J. Hydrog. Energy 48 (2023) 1582–1595.
[19] Z. Chen, M.P. Burke, Y. Ju, On the critical flame radius and minimum ignition energy for spherical flame initiation, Proc. Combust. Inst. 33 (2011) 1219–1226.
[20] C. Chi, A. Abdelsamie, D. Thévenin, Direct numerical simulations of hotspot-induced ignition in homogeneous hydrogen-air pre-mixtures and ignition spot tracking, Flow Turbul. Combust. 101 (2018) 103–121.
[21] W. Liang, C.K. Law, Z. Chen, Ignition of hydrogen/air mixtures by a heated kernel: Role of Soret diffusion, Combust. Flame 197 (2018) 416–422.
[22] H. Chu, L. Berger, T. Grenga, Z. Wu, H. Pitsch, Effects of differential diffusion on hydrogen flame kernel development under engine conditions, Proc. Combust. Inst. 39 (2023) 2129–2138.
[23] L.F.F. da Silva, B. Deshaies, M. Champion, Numerical study of ignition within hydrogen-air supersonic boundary layers, AIAA J. 31 (1993) 884–890.
[24] P. García-Ybarra, C. Treviño, Analysis of the thermal diffusion effects on the ignition of hydrogen-air mixtures in the boundary layer of a hot flat plate, Combust. Flame 96 (1994) 293–303.
[25] A. Ern, V. Giovangigli, Thermal diffusion effects in hydrogen-air and methane-air flames, Combust. Theory Model. 2 (1998) 349.
[26] R. Rajasegar, A. Srna, I. Barbery, R. Novella, On the phenomenology of hot-spot induced pre-ignition in a direct-injection hydrogen-fueled, heavy-duty, optical-engine, SAE Int. J. Adv. Curr. Pr. Mobil. 6 (2023) 1535–1547.
[27] L. De Nardi, Q. Douasbin, O. Vermorel, T. Poinsot, Infinitely fast heterogeneous catalysis model for premixed hydrogen flame-wall interaction, Combust. Flame 261 (2024) 113328.
[28] T. Falkenstein, S. Kang, L. Cai, M. Bode, H. Pitsch, DNS study of the global heat release rate during early flame kernel development under engine conditions, Combust. Flame 213 (2020) 455–466.
[29] H. Chu, L. Berger, M. Gauding, S. Pieper, H. Pitsch, Interactions of preferential diffusion and mixture inhomogeneities in hydrogen and iso-octane flame kernels under engine conditions, Combust. Flame 274 (2025) 113991.
[30] Z. Zhou, F.E. Hernández-Pérez, Y. Shoshin, J.A. van Oijen, L.P. de Goey, Effect of Soret diffusion on lean hydrogen/air flames at normal and elevated pressure and temperature, Combust. Theory Model. 21 (2017) 879–896.
[31] J. Schlup, G. Blanquart, Validation of a mixture-averaged thermal diffusion model for premixed lean hydrogen flames, Combust. Theory Model. 22 (2018) 264–290.
[32] S. Panigrahy, A.A.E.-S. Mohamed, P. Wang, G. Bourque, H.J. Curran, When hydrogen is slower than methane to ignite, Proc. Combust. Inst. 39 (2023) 253–263.
[33] B. Müller, Low-Mach-number asymptotics of the Navier-Stokes equations, J. Engrg. Math. 34 (1998) 97–109.
[34] J.O. Hirschfelder, C.F. Curtiss, R.B. Bird, The Molecular Theory of Gases and Liquids, John Wiley & Sons, 1964.
[35] N. Lamoureux, C.-E. Paillard, V. Vaslier, Low hydrocarbon mixtures ignition delay times investigation behind reflected shock waves, Shock Waves 11 (2002) 309–322.
[36] J. de Vries, J.M. Hall, S.L. Simmons, M.J. Rickard, D.M. Kalitan, E.L. Petersen, Ethane ignition and oxidation behind reflected shock waves, Combust. Flame 150 (2007) 137–150.
[37] J. Melguizo-Gavilanes, L. Boeck, R. Mével, J. Shepherd, Hot surface ignition of stoichiometric hydrogen-air mixtures, Int. J. Hydrog. Energy 42 (2017) 7393–7403.
[38] A.P. Kelley, G. Jomaas, C.K. Law, Critical radius for sustained propagation of spark-ignited spherical flames, Combust. Flame 156 (2009) 1006–1013.